Simulation of Pre-planetesimal Collisions with Smoothed Particle Hydrodynamics II

R.J. Geretshauser, F. Meru, K. Schaal, R. Speith, and W. Kley

Abstract In the frame of planet formation by coagulation the growth step from millimetre-sized highly porous dust aggregates to massive kilometre-sized planetesimals is not well constrained. In this regime of pre-planetesimals, collisional growth is endangered by disruptive collisions, disintegration by rotation as well as mutual rebound and compaction. Since laboratory studies of pre-planetesimal collisions are infeasible beyond centimetre-size, we perform numerical simulations. For this purpose, utilise the parallel smoothed particle hydrodynamics (SPH) code `parasph`. This program has been developed to simulate macroscopic highly porous dust aggregates consisting of protoplanetary material. We briefly introduce our porosity model and use it to perform simulations on the growth criteria of pre-planetesimals. With the aid of parameter studies we investigate fragmentation criteria in dust collisions depending on aggregate size and aggregate porosity. We extend a previous study on bouncing criteria of equally sized aggregates depending on their porosity and the presence of compacted shells of various porosities. Regarding the rotational stability of highly porous dust aggregates we theoretically derive fragmentation criteria for dust cylinders depending on angular velocity as well as porosity and perform suitable simulations.

R.J. Geretshauser (✉) · K. Schaal · W. Kley
Institut für Astronomie und Astrophysik, Abteilung Computational Physics, Eberhard Karls Universität Tübingen, Auf der Morgenstelle 10, 72076 Tübingen, Germany
e-mail: ralf.j.geretshauser@uni-tuebingen.de

F. Meru
Institut für Astronomie und Astrophysik, Abteilung Computational Physics, Eberhard Karls Universität Tübingen, Auf der Morgenstelle 10, 72076 Tübingen, Germany

Institut für Astronomie, ETH Zürich, Wolfgang-Pauli-Strasse 27, 8093 Zürich, Switzerland

R. Speith
Physikalisches Institut, Eberhard Karls Universität Tübingen, Auf der Morgenstelle 14, 72076 Tübingen, Germany

W.E. Nagel et al. (eds.), *High Performance Computing in Science and Engineering '12*,
DOI 10.1007/978-3-642-33374-3_6, © Springer-Verlag Berlin Heidelberg 2013

1 Introduction

According to the coagulation scenario planet formation occurs in protoplanetary discs by a sequence of successive mutual collisions from micrometre-sized dust grains to planets. Three regimes can be distinguished: during the first step from grains to millimetre-sized pre-planetesimals growth proceeds in a fractal way [5]. The growth mechanism in the second growth step from millimetre-sized pre-planetesimals to kilometre-sized planetesimals is not well constrained and subject of this work. Once a sufficient population of planetesimals exists, the third growth step to full-size planets proceeds due to gravity-aided accretion [15]. An overview of this process can be found in Ref. [9].

We turn to the second growth step from pre-planetesimals to planetesimals which is currently subject of extensive numerical and experimental effort. Two important obstacles could be identified in the pre-planetesimal regime: fragmentation and bouncing barrier. The most serious barrier is the fragmentation barrier: the relative velocities between pre-planetesimals increase as the size of the pre-planetesimals increases. The consequence is an increased probability for catastrophic disruption. Since experimental data on pre-planetesimal collisions are rather sparse, collision maps often have to contain simplistic assumptions such as a constant velocity threshold for fragmentation over several orders of magnitude in size [2, 16]. Transition velocities between parameter regions of positive and negative growth are often treated as independent from object porosities.

The second obstacle to planetesimal formation is the bouncing barrier. In this scenario [16, 28], millimetre to centimetre-sized pre-planetesimals become more and more compacted during their collisional evolution. The relative velocities for these objects are still rather low. However, due to their compact structure the pre-planetesimals rebound instead of sticking to each other or destroying each other upon collision. Recent studies indicate that if growth is halted at smaller sizes than millimetre size, the bouncing barrier could even be beneficial to planetesimal growth if some objects grow out of this barrier and sweep up all the smaller particles [27].

The need for a detailed numerical investigation of pre-planetesimal collisions arose from the lack of experimental data under realistic protoplanetary disc conditions in this field. For this reason we developed a smoothed particle hydrodynamics (SPH) code to simulate porous pre-planetesimal material [9, 11] and calibrated it with laboratory benchmark experiments [17]. For a detailed classification of the collision outcome we developed the four-population model [10]. Numerical model and classification scheme were utilised to show that the stability of pre-planetesimals is significantly decreased if they possess an inhomogeneous structure [12, 13]. Additionally, preliminary studies showed that the conditions for rebound are drastically changed if pre-planetesimals feature a compacted outer shell [9, 13]. We also begun with a large-scale parameter study of pre-planetesimal collisions in the decimetre regime which already indicated that size ratio and porosity of the collision partners have an influence on the collision outcome, which is not negligible [9, 13].

In this article we continue this work. Initially, in Sect. 2, we briefly review the code and porosity model. Detailed quantitative investigations of size- and porosity-dependence of the fragmentation velocity threshold are presented in Sect. 3.1. The influence of the compactness of hard shells is studied in Sect. 3.2. Finally, in Sect. 3.3, analytical formulae for the stability of rotating dust aggregates are presented and counterchecked with simulations. Further areas of research are described in the outlook Sect. 4.

2 SPH Code and Porosity Model

2.1 Solid Body SPH

For the simulation of pre-planetesimal collisions we utilise the numerical method *smoothed particle hydrodynamics (SPH)* [14,21] together with extensions for solid body mechanics [1,20,22] and a suitable porosity model [11,25].

As a method which was originally developed for pure hydrodynamics, SPH relies on the usual equations of continuum mechnics to ensure conservation of mass, momentum, and energy. Under external forces, stresses develop inside a solid body to restore its original shape. Hence, the main properties of solid body mechanics enter in the momentum equation via the stress tensor $\sigma_{\alpha\beta}$, which is defined as

$$\sigma_{\alpha\beta} = -p\delta_{\alpha\beta} + S_{\alpha\beta} \ , \tag{1}$$

where p and $S_{\alpha\beta}$ denote the hydrostatic pressure and deviatoric stress tensor, respectively. Throughout this article Greek indices denote the spatial components and the Einstein summing notation is applied. The time evolution of the deviatoric stress tensor is computed according to Hooke's law in frame invariant Jaumann rate form [1,9,11,13,24]. The transition to plastic deformation due to shear is determined by the von Mises criterion

$$S^{\alpha\beta} \rightarrow f S^{\alpha\beta}, \tag{2}$$

where $f = \min\left[Y^2(\phi)/3J_2, 1\right]$ and $Y = Y(\phi)$ is the shear strength. The quantity $J_2 = S_{\alpha\beta}S_{\alpha\beta}$ is the second irreducible invariant of the deviatoric stress tensor. Subgrid porosity is modelled by the filling factor ϕ, which is defined as

$$\phi = \frac{\rho}{\rho_\mathrm{s}} = 1 - \Phi \ , \tag{3}$$

where ρ, ρ_s, and Φ are the density of the porous material, the density of the matrix material, and the porosity, respectively. The pre-planetesimal material is monodisperse spherical SiO_2 dust [3,4] dust for which $\rho_\mathrm{s} = 2,000\,\mathrm{kg\,m^{-3}}$.

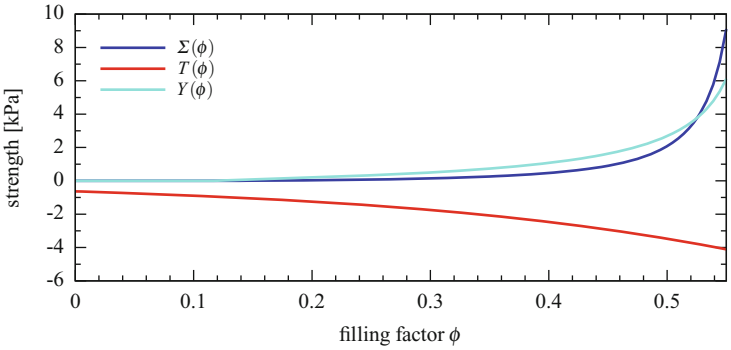

Fig. 1 Calibrated strength curves. The compressive strength $\Sigma(\phi)$, tensile strength $T(\phi)$, and shear strength $Y(\phi)$ as a result of the calibration process described in Ref. [11]

The elastic as well as the plastic evolution of the hydrostatic part of the stress tensor are computed according to the filling-factor-dependent bulk modulus $K(\phi)$ as well as the compressive strength $\Sigma(\phi)$ and tensile strength $T(\phi)$ [11–13], respectively. The bulk modulus scales with the filling factor by the following relation

$$K(\phi) = K_0 \left(\frac{\phi}{\phi_{\text{RBD}}} \right)^{\gamma} \tag{4}$$

where $\gamma = 4$ and K_0 is the bulk modulus of an uncompressed random ballistic deposition (RBD) dust sample with $\phi_{\text{RBD}} = 0.15$ [3]. This value was calibrated to be $K_0 = K(\phi_{\text{RBD}}) = 4.5\,\text{kPa}$ [11].

The strength quantities [11, 17] are illustrated in Fig. 1 and represent transition thresholds from the elastic to the plastic regime. The tensile strength is given by a power-law

$$T(\phi) = -10^{2.8+1.48\phi}\,\text{Pa}\,. \tag{5}$$

The compressive strength takes the form

$$\Sigma(\phi) = p_{\text{m}} \left(\frac{\phi_{\text{max}} - \phi_{\text{min}}}{\phi_{\text{max}} - \phi} - 1 \right)^{\Delta \ln 10}, \tag{6}$$

with $\phi_{\text{max}} = 0.58$ and $\phi_{\text{min}} = 0.12$, which denote maximum and minimum filling factor of the compressive strength relation. The quantity $\Delta \ln 10$ is the power of the expression with $\Delta = 0.58$. The constant $p_{\text{m}} = 260\,\text{Pa}$ is its mean pressure.

The shear strength is given by the geometric mean of Eqs. (5) and (6)

$$Y(\phi) = \sqrt{\Sigma(\phi)|T(\phi)|}\,. \tag{7}$$

2.2 *The Code* `Parasph`

The `parasph` code was developed by Hipp [19] and extended by Schäfer for the simulation of ductile, brittle, and porous media [23, 24]. The porosity model was improved and calibrated by Geretshauser for pre-planetesimal material [9, 11] together with other extensions. The program is based on the `parasph` library [6,7]. This is a set of routines developed for a easier and faster handling of parallel particle codes. By means of this library the physical problem and the parallel implementation are clearly separated. `parasph` features domain decomposition, load balancing, nearest neighbour search, and inter-node communication. Moreover, SPH enhancements such as additional artificial stress and XSPH were implemented. The adaptive Runge-Kutta-Cash-Karp integrator has been used for the simulations presented here. For testing purposes an adaptive second order Runge-Kutta, and an Euler integrator was added. HDF5 (Hierarchical Data Format) was included as a compressed input and output file format with increased accuracy, which decreases the amount of required storage space considerably. The parallel implementation utilises the Message Passing Interface (MPI) library. Test simulations yielded a speedup of 120 on 256 single core processors of a Cray T3E and of 60 on 128 single core processors on a Beowulf-Cluster.

3 Results

The simulations in this section are carried out with 240,143–476,476 SPH particles depending on the size of the projectile. The program `parasph` is run on the NEC Nehalem cluster of the HLRS. Depending on the size of the problem 32–80 cores were used. The simulation time is strongly dependent on the collision velocity. In particular for fragmenting collisions the adaptive time step becomes as small as $\sim 10^{-5}$ s throughout the whole simulation. In contrast in bouncing and sticking collisions, the time step is initially low and than increases for the rest of the simulation. To give a rough number, simulations take 72–240 h wall-clock time for 1 s of simulated time depending on size of the problem and involved physical process.

3.1 *Velocity Thresholds*

The main focus of the project lies on the investigation of the growth conditions for macroscopic pre-planetesimals. In this section we carry out simulations to constrain the influence of projectile size and aggregate porosity on these conditions for centimetre to decimetre-sized pre-planetesimals. Although the velocity threshold

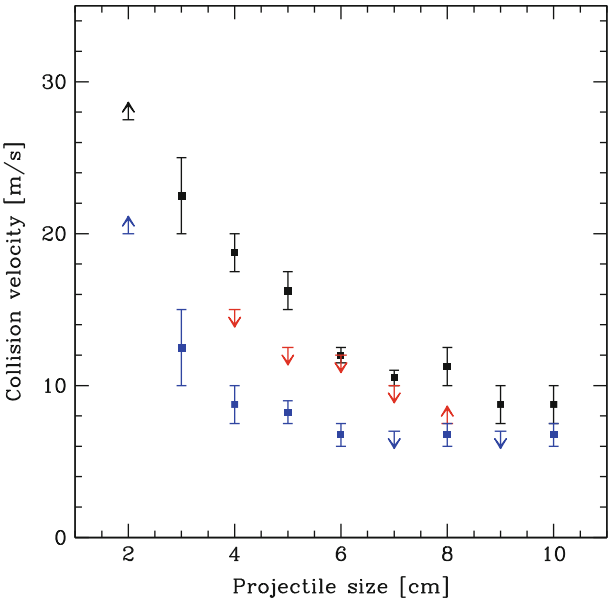

Fig. 2 Fragmentation threshold velocity against projectile size. The different colours represent the filling factors $\phi = 0.15$ (*blue*), $\phi = 0.25$ (*red*), and $\phi = 0.35$ (*black*). The *arrows* denote *upper* and *lower* limits. The target is a sphere of radius 10 cm. Due to the higher collision energy the threshold velocity for fragmentation decreases with increasing projectile size. Highly porous aggregates ($\phi = 0.15$) are less stable than aggregates of intermediate porosity ($\phi = 0.35$)

for fragmentation might be significantly lowered if the pre-planetesimals possess an inhomogeneous filling factor distribution [10], we restrain to initially homogeneous aggregates as a simplification and reference case.

Figure 2 illustrates the dependence of the fragmentation threshold velocity on the size of the impacting projectile. In each case the target is a porous dust sphere of radius 10 cm. Also the projectile has spherical shape. Both objects are homogeneous and of identical filling factor. We investigate three of the latter: $\phi = 0.15$, $\phi = 0.25$, and $\phi = 0.35$. This represents a range between high and intermediate porosity. All three curves have a similar shape. Very small projectiles intrude into the target and get swallowed. Only few dust fragments are ejected. With increasing projectile size the impact energy increases and hence the threshold for disruption decreases. However, compared to the immense range of sizes in pre-planetesimal collisions ranging from millimetre to kilometre sizes the difference in threshold fragmentation velocity within the quite narrow investigated size range is remarkable. We conclude that even small differences in size have to be considered in the field of pre-planetesimal growth. Figure 2 already gives rise to another important dependence: the aggregate porosity.

Figure 3 shows a surprising dependence of the threshold velocity on the aggregate porosity. As a standard setup for this study we collide two homogeneous

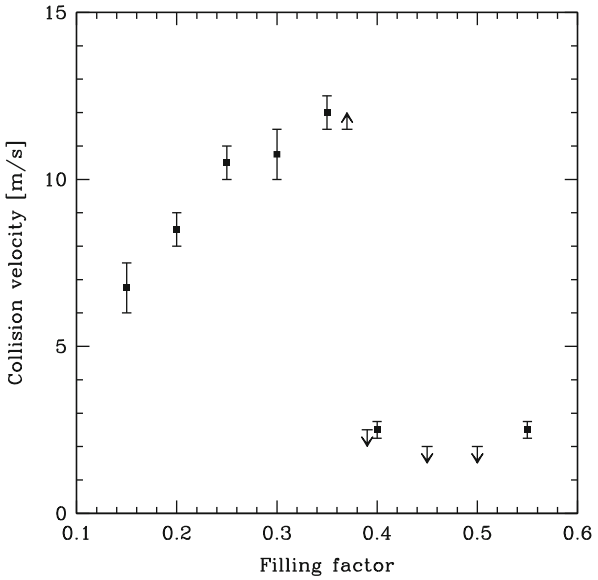

Fig. 3 Threshold velocity for fragmentation against filling factor. The target and projectile are spheres of radius 10 cm and 6 cm, respectively. The *arrows* denote *upper* and *lower* limits. Starting from low filling factors the threshold velocity increases because the strength of the aggregate increases. At a filling factor of $\phi \sim 0.37$ a sharp drop occurs

spherical aggregates with vanishing impact parameter. The target and projectile radii are 10 cm and 6 cm, respectively. At low filling factors or, equivalently, high porosity, the tensile and shear strength are low (see Eqs. (5), (7), and Fig. 1). As a consequence, such pre-planetesimals are rather fragile. However, the compressive strength is also rather low (Eq. (6) and Fig. 1) and hence energy can easily be dissipated by plastic deformation since the pressure threshold for plastic compression is exceeded in each collision.

As the filling factor increases the compressive strength, shear strength, and tensile strength increase. On the one hand the plastic deformability of the aggregate and hence the ability to dissipate energy hereby decrease. On the other hand, however, the aggregates become less fragile. Overall the aggregates gain a higher stability and the threshold velocity further increases for higher filling factors.

At a filling factor of $\phi \sim 0.35$ a sudden drop in the threshold velocity occurs. This drop is surprising and is caused by a complex interplay between the elastic and plastic properties of the aggregates which makes it difficult to capture this feature quantitatively. This issue is still object of ongoing research but the influence of the following aspects could be identified. (1) With increasing compressive strength $Y(\phi)$ an increasing fraction of the initial kinetic energy can be stored in elastic loading of the aggregates (see also Sect. 3.2). As a consequence, this elastic energy is available for the separation of the aggregates in a bouncing collision. (2) With increasing ϕ also the bulk modulus of the aggregates increases (Eq. (4)) and the

aggregates become stiffer. As a result, the contact area between the aggregates decreases and less energy is necessary to separate the aggregates in a bouncing collision. (3) Because of partial sticking of the aggregates, a clean growth-neutral bouncing is unrealistic. Instead some mass transfer or even the rip out of larger chunks can be expected. (4) Due to the increase in $\Sigma(\phi)$ and $K(\phi)$ density waves of increasing amplitude propagate across the aggregate and lead to a local rarefaction of the material and consequential local reduction of shear and tensile strength (see also a similar phenomenon in Sect. 3.3). These density waves finally rip the aggregate apart even at low collision velocities.

The aspects (1) and (2) decrease the probability for sticking of the projectile to the target and increase the probability of bouncing of the targets. Aspect (4) increases the probability for fragmentation of the aggregate. The collisions at the drop of the threshold velocity in Fig. 3 show a behaviour where the aggregates mainly bounce but partly also fragment or some mass transfer (aspect 3) occurs. Since sticking and consequential growth and bouncing (with some fragmentation or mass transfer), resulting in neutral or negative growth, are two clearly distinct physical processes, a sharp drop in the describing threshold velocity can be expected which at least qualitatively explains the shape of the curve in Fig. 3. We note that a collision model based on experimental data [16] which features only the categories "porous" and "compact" aggregates uses a filling factor of $\phi = 0.40$ as separation criterion which is close to the drop filling factor of $\phi = 0.37$. Other experimental investigations [26] find that the maximum filling factor that can be reached for porous aggregates in protoplanetary discs is roughly $\phi \sim 0.33$. However, this value is obtained for polydisperse SiO_2 dust which is less compressible. This value can be expected to be higher for our monodisperse dust. To summarise, the drop in our threshold velocity curve occurs where also experimental data indicate a significant change in the collision behaviour of dust aggregates. However, the reasons for this drop require a closer investigation.

3.2 Bouncing, Hard Shells and Porosity

In our first study we investigate the influence of porosity on the bouncing and sticking behaviour. This is to assess whether the experiments with intermediate porosity [2] and high porosity [18] can be combined into the collision map presented by Güttler et al. [16].

For this, we conduct simulations of collisions between a homogeneous target and projectile. We distinguish three cases where both objects feature a uniform filling factor of $\phi = 0.15$, $\phi = 0.35$, and $\phi = 0.55$. According to the compressive strength relation this is nearly equivalent to maximum, intermediate, and minimum porosity. The aggregates thus feature very low, intermediate, and very high pressure thresholds for plastic deformation. Resulting from this property we expect a strong dependence of the filling factor on the sticking and bouncing behavior. The

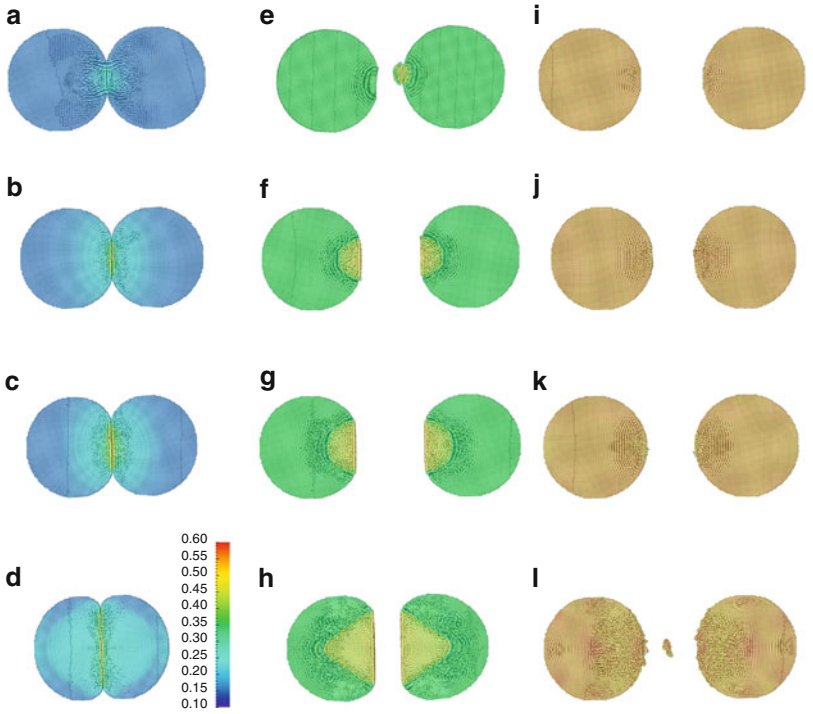

Fig. 4 Cross-section through the outcome of collision simulations with homogeneous aggregates for high ($\phi_i = 0.15$, *left*), intermediate ($\phi_i = 0.35$, *middle*) and low porosity ($\phi_i = 0.55$, *right*). The projectile radius is equal to the target radius. The collision velocities are in the first line (*a, e, i*) 0.1, in the second line (*b, f, j*) 0.3, in the third line (*c, g, k*) 0.5, and in the fourth line (*d, h, l*) 1.0 ms^{-1}. The highly porous dust aggregates stick for each of the simulated collision velocities. The filling factor is increased in the vicinity of the impact site. Additionally the aggregates are deformed to almost kidney shape for 1.0 ms^{-1} (*d*). In contrast, the homogeneous aggregates with $\phi_i = 0.35$ exclusively rebound. The region of increased filling factor in the interior increases with collision velocity. The impact site is flattened. The aggregates with low filling factor also exclusively rebound at the given velocities. However, no significant compaction or deformation is visible except some fragmentation for the highest collision velocity (*l*)

impacting projectile has a radius $r_p = 10$ cm just like the target. The impact velocity v_0 is 0.1, 0.3, 0.5, and 1.0 ms^{-1}.

The theoretical demarcation between sticking and bouncing in Ref. [16] makes the following assumptions: (1) elastic deformation of the aggregates, and (2) the filling factor in the contact region is not changed in the collision. These assumptions are too simplistic.

1. The assumption of elastic deformation of the aggregates is only valid for filling factors close to the maximum filling factor. In particular for highly porous aggregates the deformation is highly plastic and as a consequence the contact area between the aggregates is increased compared to elastic contact (see e.g. Fig. 4d).

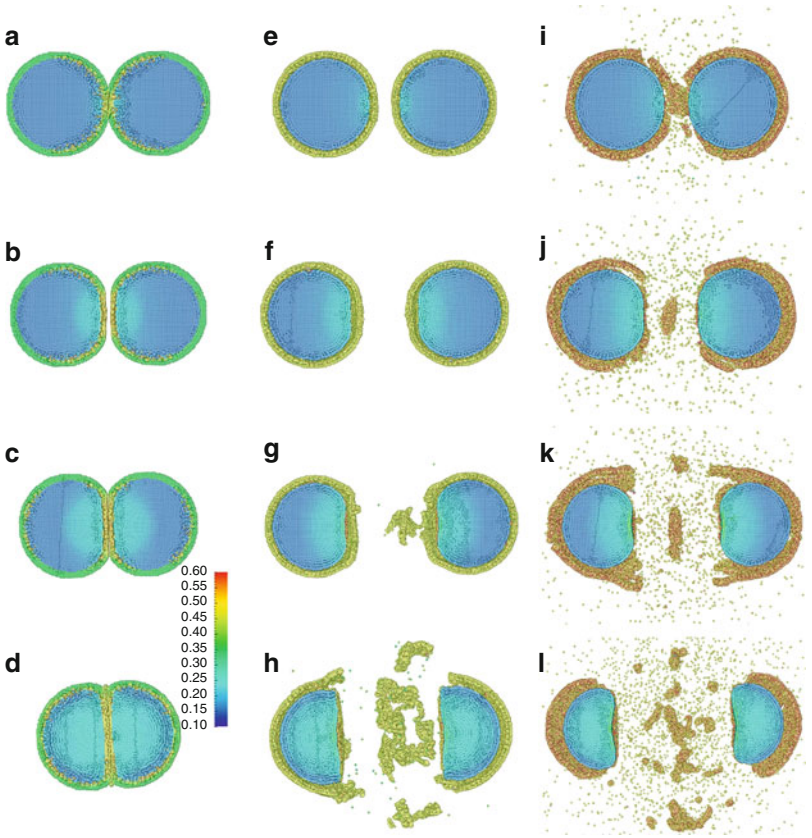

Fig. 5 Cross-section through collision results involving aggregates with a hard shell of 0.1 r. The interior of all aggregates is highly porous $\phi_c = 0.15$, which would lead to perfect sticking if the aggregates were homogeneous. However, in the *left* (*a–d*), *middle* (*e–h*), and *right column* (*i–l*) the filling factors of the hard shell are 0.35, 0.45, and 0.55, respectively. Initially, both aggregates are spheres of 10 cm radius. The displayed cross-sections show the situation after the impact with 0.1 (*a, e, i*), 0.3 (*b, f, g*), 0.5 (*c, g, k*), and 1.0 ms^{-1} (*d, h, l*). Even thin hard shells can lead to bouncing if the filling factor is sufficiently high

2. As it can clearly be seen in Fig. 4, the filling factor is highly increased in the contact area. This leads to an increased tensile strength in this region (Eq. (5)). An increased tensile strength, however, also increases the contact energy, which promotes sticking.

We conclude, that because of these effects in particular for highly porous dust aggregates the threshold velocity for sticking is much larger than presented in [16]. Consequently, the parameter space where bouncing occurs is much smaller than assumed in this reference and sticking dominates for low velocities and low filling factors.

We use the same setup as above regarding ratio of target and projectile radius and collision velocity, but we add a hard outer shell (Fig. 5). The thickness of the hard shell is given as a fixed fraction of target and projectile radii, respectively, i.e. 0.1, 0.2, 0.3, 0.4. The core of all aggregates has a filling factor $\phi_c = 0.15$, whereas the filling factor of the hard shell ϕ_h takes the values 0.35, 0.45, and 0.55.

From the comparison with aggregates without hard shell, which exclusively resulted in sticking (cf. Fig. 4, first row), it is evident that hard shells do have an influence on the bouncing behaviour of dust aggregates. This is because for aggregates with $\phi = 0.15$ the compressive strength is very low. As a consequence, nearly the total kinetic energy of the impact is dissipated by plastic deformation and nearly no elastic loading of the colliding objects is possible.

Conversely, for aggregates with hard shells ($\phi_h = 0.35$) the plastic deformation threshold is higher for the shell. During the impact, the shell is elastically loaded and the aggregates rebound. However, in the immediate area around the impact site the deformation threshold for the shell is exceeded and plastic deformation takes place in the hard shell. Therefore, the tensile $T(\phi)$ and shear $Y(\phi)$ strengths are increased in this region and counteract the bouncing. However, hard shells of intermediate porosity are still sufficiently plastically deformable such that bouncing is still a rare event in the investigated parameter space.

The situation changes for hard shell filling factors of $\phi_h = 0.45$ and 0.55. The value of $\phi_h = 0.55$ is close to maximum compaction. Thus, the hard shell rather breaks than being plastically deformed. As a consequence of the lacking plastic deformability the collisions of aggregates with denser hard shells exclusively result in bouncing and partial fragmentation (of the shell).

We conclude that hard shells of intermediate porosity in general do not prevent sticking. Only in a few cases, where the hard shell was thick enough for sufficient elastic loading or at the right velocity for a thin hard shell bouncing occurs. However, if the hard shells become more compact, even thin shells suffice to yield bouncing collisions. For very compact hard shells and higher collision velocities partial fragmentation of mostly shell material can be expected.

3.3 Stability of Rotating Dust Aggregates

Particularly in aggregate collisions where the impact parameter is not vanishing, the aggregates or fragments start to rotate [24]. However, high spinning rates may lead to additional disruption of the aggregates since tidal forces may tear them apart. To assess this effect for pre-planetesimal collisions, we analytically derive critical angular velocities for a long rotating dust cylinder depending on its filling factor and radius. Additionally we carry out simulations of rotating cylinders with the same specifications. As a consistency check of the SPH code we compare the stress evolution inside the cylinder with the theoretical reference. We also compare the simulated critical angular velocity with the expected value.

Table 1 Results of the rotating cylinder study. The cylinders have an initial filling factor ϕ_i. The rotation is accelerated by $\dot{\omega}$. The onset of fragmentation starts at a critical time t_c and a critical angular velocity ω_c. Simulated and theoretical value of the latter are compared

ϕ_i	$\dot{\omega}[s^{-1}]$	$t_c[s]$	$\omega_c[s^{-1}]$ simulation	$\omega_c[s]$ theory	%
0.15	1	9.95	9.64	9.52	101.26
0.25	1	10.2	9.86	14.3	68.95
0.35	0.2	31.25	6.08	17.98	33.82
0.45	0.2	28.4	5.50	23.56	23.34
0.55	0.2	27.05	5.20	34.36	15.13

According to our porosity model presented in Sect. 2 disruption can occur when the stress inside the cylinder represented by the full stress tensor $\sigma_{\alpha\beta}$ exceeds either the tensile strength $T(\phi)$ or the shear strength $Y(\phi)$. For each angular velocity ω the stress state is well defined [8]. From this one can derive two critical angular velocities ω_c^T and ω_c^Y. The first arises from the tensile strength criterion and reads:

$$\omega_c^T = \sqrt{\frac{-12(1-\nu)}{\rho_0 r_0^2 (3-\nu)} T(\phi)}\,, \tag{8}$$

where r_0 and ν are the radius of the cylinder and the Poisson ratio, respectively. Fragmentation due to exceeding the shear strength occurs when the following critical angular velocity is reached

$$\omega_c^Y = \sqrt{\frac{8(1-\nu)}{\rho_0 r_0^2 (3-4\nu)} Y(\phi)}. \tag{9}$$

The cylinder fragments at the minimum of one of these velocities. The theoretical values for the fragmentation criterion can be found in Table 1 for the investigated initial filling factors ϕ_i.

To check our theoretical predictions, we carry out simulations of a rotating cylinder consisting of porous SiO_2 dust. The radius of the cylinder is $r_0 = 10\,\text{cm}$ and its height is $h = 60\,\text{cm}$. It rotates about the z-axis which represents the central axis of the cylinder and is accelerated by an constant angular acceleration $\dot{\omega}$. The exact values are given in Table 1.

Initially the cylinder deforms elastically and the tensions inside the body increase. We measure the principal stresses of $\sigma_{\alpha\beta}$ along a line from (0,0,0) which represents the centre of mass of the cylinder radially outwards along the x-axis. The resulting principal stresses in cylinder coordinates $\sigma_{\phi\phi}$, σ_{rr} and σ_{zz} are displayed in Fig. 6 for $t = 10\,\text{s}$ and $t = 25\,\text{s}$, shortly before the cylinder fragments. During its whole elastic evolution the stresses match the theoretical predictions extremely well. This confirms the validity of our code in the elastic regime.

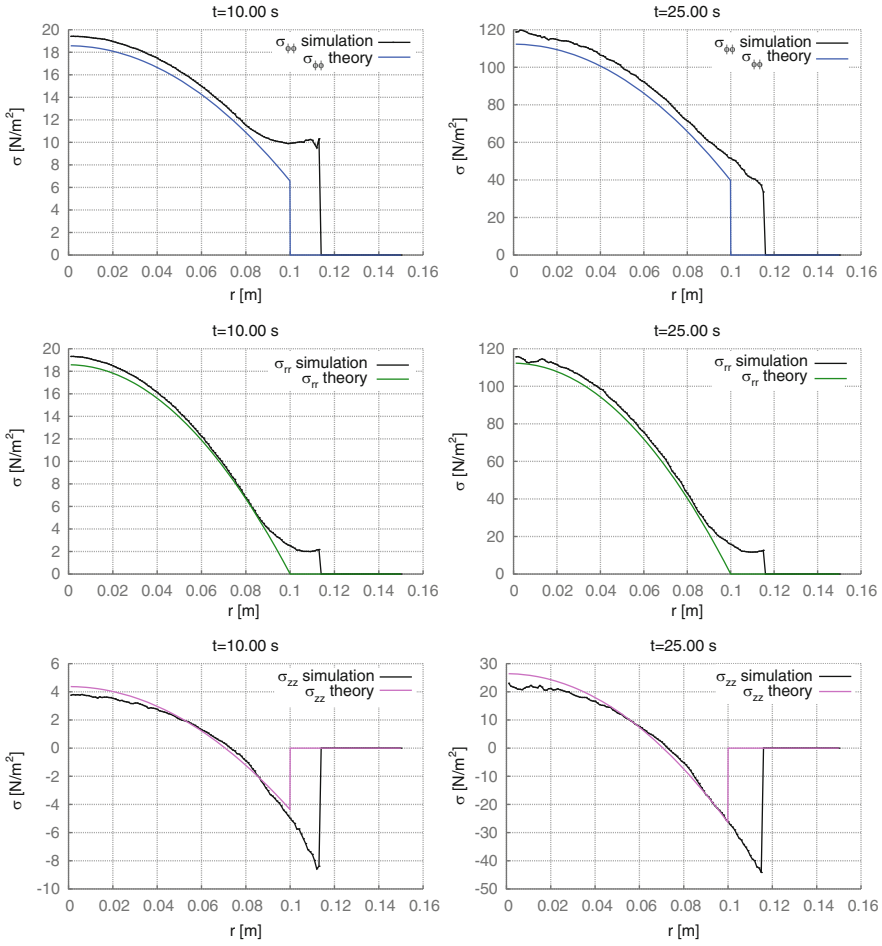

Fig. 6 Stresses $\sigma_{\alpha\beta}$ of the stable rotating cylinder with $\phi_\mathrm{i} = 0.55$. The principal stresses in cylinder coordinates $\sigma_{\phi\phi}$ (*top*), σ_{rr} (*middle*), and σ_{zz} are measured along a line from the centre of the cylinder radially outwards at two different times $t = 10\,\mathrm{s}$ (*left*) and $t = 25\,\mathrm{s}$ (*right*). In this elastic regime the simulated stresses (*black*) almost perfectly follow the curves expected from the theory (*colored*). The radius of the cylinder is 10 cm, however due to SPH smoothing this boundary is exceeded in the graphs. At the rim the stresses start to deviate from the expected values

With respect to fragmentation, the simulation for the cylinder with $\phi_\mathrm{i} = 0.15$ reproduces the critical angular velocity very well (see Table 1). For higher initial filling factors however, the predicted critical angular velocity is much larger than the simulated value. The discrepancy increases with ϕ_i. The reason for this is illustrated in Fig. 7 which displays the evolution of the density inside the cylinder. As the body rotates density waves develop inside. These lead to a local rarefaction of the material. As a consequence the tensile and shear strength is diminished in these

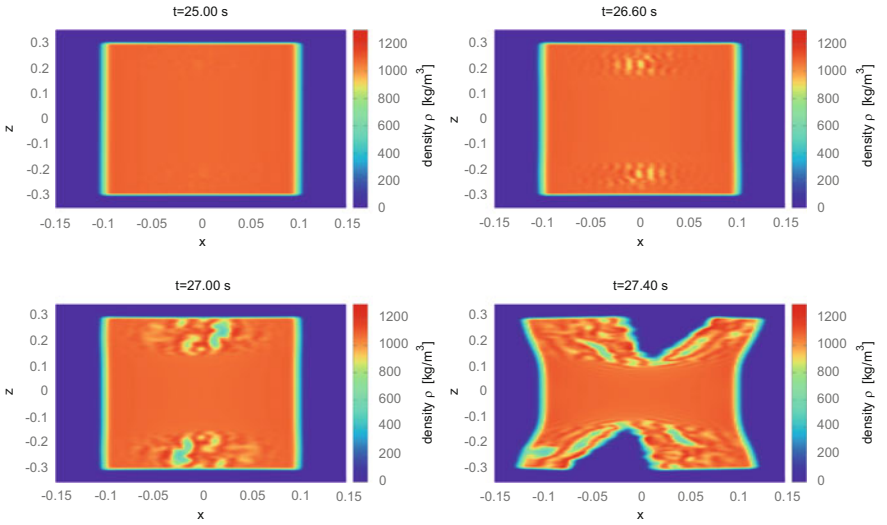

Fig. 7 Density evolution of a rotating cylinder with $\phi_i = 0.55$ after the stable phase. The images show a cut along the x-z plane through the centre of the cylinder which is rotating about the z-axis. The density is colour-coded. While at $t = 25$ s the density distribution is still homogeneous, at $t = 26$ s density fluctuations at the *top* and *bottom* of the cylinder start to develop. Together with the density the tensile and shear strength are locally diminished. These regions are weak spots at which rupture starts ($t = 27$ s and $t = 27.4$ s)

regions (Fig. 8). However, the stresses increase with increasing angular velocity. The rarefied regions serve as weak spots from which rupture can develop due to material failure which arises from a stress exceeding the strength values.

4 Outlook

The presented results encourage further studies for a deeper insight into the outcome of pre-planetesimal collisions. First of all, the sudden drop in fragmentation threshold velocity at a given porosity requires further investigations. More simulations have to be carried out to assess other dependencies of this behaviour, for example the projectile size. A high resolution in time is desirable at this transition point to understand the complex interplay between elastic and plastic behaviour. With respect to the rotating cylinder the development of the elastic waves should be studied in more detail.

Recently, new measurements for another possible pre-planetesimal material became available. This demands for an extensive parameter study using this new material to explore possible differences with respect to growth conditions. Off-centre collisions of pre-planetesimals are still a desiderate because they represent the more realistic situation in the disc.

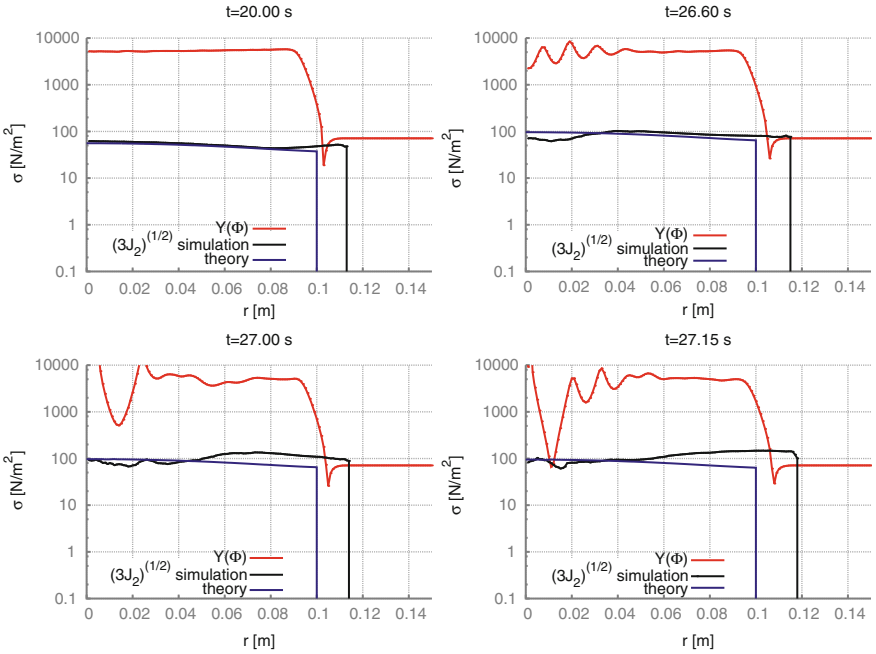

Fig. 8 Local shear strength $Y(\phi)$ (*red*) and von Mises stress $\sqrt{3J_2}$ (*black*) for $r > 0$ at $z = 0.2$ for a rotating cylinder with $\phi_i = 0.55$. According to the von Mises yielding criterion the cylinder starts to fragment once the von Mises stress exceeds the shear strength. In the stable regime ($t = 20\,\mathrm{s}$) $Y(\phi)$ is two magnitudes larger than the stresses. However, density fluctuations lead also to fluctuations in $Y(\phi)$ which are already visible at $t = 26\,\mathrm{s}$ and $t = 27\,\mathrm{s}$. Eventually, the shear strength locally falls below the von Mises stress at $t = 27.15\,\mathrm{s}$ and $r \sim 1\,\mathrm{cm}$ and rupture sets in

To gain an idea of what realistic processed pre-planetesimals look like, it is desirable to study the collision history of an aggregate. For this, a homogeneous aggregate is subsequently collided with other aggregates of different sizes and filling factor at various collision velocities. The input information for a realistic collision sequence can be derived from global coagulation simulations.

References

1. Benz, W., Asphaug, E.: Impact Simulations with Fracture. I. Method and Tests. Icarus **107**(1), 98–116 (1994)
2. Blum, J., Münch, M.: Experimental Investigations on Aggregate-Aggregate Collisions in the Early Solar Nebula. Icarus **106**(1), 151–167 (1993)
3. Blum, J., Schräpler, R.: Structure and Mechanical Properties of High-Porosity Macroscopic Agglomerates Formed by Random Ballistic Deposition. Phys. Rev. Lett. **93**(11), 115,503 (2004)

4. Blum, J., Schräpler, R., Davidsson, B.J.R., Trigo-Rodriguez, J.M.: The Physics of Protoplanetesimal Dust Agglomerates. I. Mechanical Properties and Relations to Primitive Bodies in the Solar System. The Astrophysical Journal **652**(2), 1768–1781 (2006)
5. Blum, J., Wurm, G.: The Growth Mechanisms of Macroscopic Bodies in Protoplanetary Disks. Annual Review of Astronomy and Astrophysics **46**(1), 21–56 (2008)
6. Bubeck, T., Hipp, M., Hüttemann, S., Kunze, S., Ritt, M., Rosenstiel, W., Ruder, H., Speith, R.: Parallel SPH on Cray T3E and NEC SX-4 using DTS. In: E. Krause, W. Jäger (eds.) High performance computing in science and engineering '98, pp. 396–410. Springer, Berlin and and New York (1999)
7. Bubeck, T., Hipp, M., Hüttmann, S., Kunze, S., Ritt, M., Rosenstiel, W., Ruder, H., Speith, R.: SPH test simulations on a portable parallel environment. In: Proceedings of the Workshop on Physics and Computer Science, pp. 139–155 (1999)
8. Chakrabarty, J.: Theory of plasticity, 3 edn. Elsevier/Butterworth-Heinemann, Amsterdam and and Boston and and Oxford (2006)
9. Geretshauser, R.J.: Simulation of pre-planetesimal collisions with smoothed particle hydrodynamics. Ph.D. thesis, Universität Tübingen, Tübingen (2011)
10. Geretshauser, R.J., Meru, F., Speith, R., Kley, W.: The four-population model: a new classification scheme for pre-planetesimal collisions. Astronomy & Astrophysics **531**, A166 (2011)
11. Geretshauser, R.J., Speith, R., Güttler, C., Krause, M., Blum, J.: Numerical simulations of highly porous dust aggregates in the low-velocity collision regime: Implementation and calibration of a smooth particle hydrodynamics code. Astronomy and Astrophysics **513**, A58 (2010)
12. Geretshauser, R.J., Speith, R., Kley, W.: Collisions of inhomogeneous pre-planetesimals. Astronomy & Astrophysics **536**, A104 (2011)
13. Geretshauser, R.J., Speith, R., Kley, W.: Simulation of Pre-Planetesimal Collisions with Smoothed Particle Hydrodynamics. In: W.E. Nagel, D.B. Kröner, M. Resch (eds.) High performance computing in science and engineering '11, pp. 29–45. Springer, Berlin and New York (2012)
14. Gingold, R.A., Monaghan, J.J.: Smoothed particle hydrodynamics – Theory and application to non-spherical stars. Monthly Notices of the Royal Astronomical Society **181**, 375–389 (1977)
15. Goldreich, P., Lithwick, Y., Sari, R.: Final Stages of Planet Formation. The Astrophysical Journal **614**(1), 497 (2004)
16. Güttler, C., Blum, J., Zsom, A., Ormel, C.W., Dullemond, C.P.: The outcome of protoplanetary dust growth: pebbles, boulders, or planetesimals? - I. Mapping the zoo of laboratory collision experiments. Astronomy and Astrophysics **513**, A56 (2010)
17. Güttler, C., Krause, M., Geretshauser, R.J., Speith, R., Blum, J.: The Physics of Protoplanetesimal Dust Agglomerates. IV. Toward a Dynamical Collision Model. The Astrophysical Journal **701**, 130–141 (2009)
18. Heißelmann, D., Fraser, H.J., Blum, J.: Experimental Studies on the Aggregation Properties of Ice and Dust in Planet-Forming Regions. International Astronautical Congress Abstracts **58**, 1–6 (2007)
19. Hipp, M., Rosenstiel, W.: Parallel hybrid particle simulations using mpi and openmp. In: M. Danelutto, D. Laforenza, M. Vanneschi (eds.) Euro Par 2004 parallel processing, pp. 189–197. Springer (2004)
20. Libersky, L.D., Petschek, A.G.: Smooth Particle Hydrodynamics with Stength of Materials. In: H. Trease, M.J. Fritts, W.P. Crowley (eds.) Advances in the Free-Lagrange method: including contributions on adaptive gridding and the smooth particle hydrodynamics method, *Lecture notes in physics*, vol. 395. Springer (1991)
21. Lucy, L.B.: A numerical approach to the testing of the fission hypothesis. The Astronomical Journal **82**, 1013–1024 (1977)
22. Randles, P.W., Libersky, L.D.: Smoothed Particle Hydrodynamics: Some recent improvements and applications. Computer Methods in Applied Mechanics and Engineering **139**(1–4), 375–408 (1996)

23. Schäfer, C.: Application of Smooth Particle Hydrodynamics to selected Aspects of Planet Formation. Ph.D. thesis, Universität Tübingen, Tübingen (2005)
24. Schäfer, C., Speith, R., Kley, W.: Collisions between equal-sized ice grain agglomerates. Astronomy and Astrophysics **470**(2), 733–739 (2007)
25. Sirono, S.: Conditions for collisional growth of a grain aggregate. Icarus **167**(2), 431–452 (2004)
26. Teiser, J., Engelhardt, I., Wurm, G.: Porosities of Protoplanetary Dust Agglomerates from Collision Experiments. The Astrophysical Journal **742**(1), 5 (2011)
27. Windmark, F., Birnstiel, T., Güttler, C., Blum, J., Dullemond, C.P., Henning, T.: Planetesimal formation by sweep-up: how the bouncing barrier can be beneficial to growth. Astronomy and Astrophysics **540**, A73 (2012)
28. Zsom, A., Ormel, C.W., Güttler C., Blum, J., Dullemond, C.P.: The outcome of protoplanetary dust growth: pebbles, boulders, or planetesimals? II. Introducing the bouncing barrier. Astronomy and Astrophysics **513**, A57 (2010)